Electron Microscopy, Neutron Diffraction, and Physical Properties of $Bi_4Sr_8Cu_5O_{19+y}$

M. T. Caldes, J. M. Navarro, F. Perez, M. Carrera, J. Fontcuberta, N. Casan-Pastor, C. Miravitlles, X. Obradors, J. Rodriguez-Carvajal,† J. M. Gonzalez-Calbet,‡ M. Vallet-Regi,‡ A. Garcia,‡ and A. Fuertes*

Institut de Ciencia de Materials de Barcelona, Campus U.A.B., 08193 Bellaterra, Barcelona, Spain

Received March 4, 1991. Revised Manuscript Received May 30, 1991

The preparation and study of the structural and physical properties of the so-called *tubular-phase* $Bi_4Sr_8Cu_5O_{19+y}$ by neutron powder diffraction, high-resolution electron microscopy, electrical resistivity, and magnetic susceptibility measurements are reported. This oxide is closely related structurally to the $n = 1$ bismuth cuprate superconductor $Bi_2Sr_2CuO_{6+y}$, differing by the presence of extra Sr–Cu–Sr perovskite layers perpendicular to the $[CuO_2]$ planes. Neutron powder diffraction results are essentially in agreement with previous structural refinements based on single-crystal X-ray diffraction data. The structure is described in the space group *Fmmm* with the oxygen atoms in the bismuth planes appearing disordered at intermediate positions between NaCl and bridging sites as occurs for superconductors in the family $Bi_2Sr_2Ca_{n-1}Cu_nO_{2n+4}$. Electron diffraction patterns and HREM images show that such disorder does not lead to the existence of a structural modulation as in the above family: The extra Sr–Cu–Sr perovskite layers perpendicular to the $[CuO_2]$ planes convert the layered $Bi_2Sr_2CuO_{6+y}$ structure into a rigid network, preventing the corrugation of the slabs and the modulation of the structure. Calculations based on Brown's method show a heterogeneous charge distribution among copper ions. Study of powder neutron diffraction patterns between 1.5 and 998 K does not show either any relevant structural change nor evidence of 3D antiferromagnetic ordering. Electrical resistivity measurements in the $60\ K \leq T \leq 300\ K$ temperature range indicate semiconducting behavior. The observed magnetic susceptibility is consistent with the existence of paramagnetic defects within a 2D strongly correlated antiferromagnetism.

Introduction

The discovery of superconductivity at 20 K in the Bi–Sr–Cu–O system by Michel et al.[1] and later in the Bi–Sr–Ca–Cu–O system at temperatures above 100 K[2-6] has developed a strong interest in the search for new phases that could exist in these systems. Within the family of Bi–Sr–Cu ternary oxides, two phases have been well characterized so far. First, the superconducting oxide $Bi_2Sr_2CuO_{6+y}$, which is the $n = 1$ member of the series $Bi_2Sr_2Ca_{n-1}Cu_nO_{2n+4}$ with a value of T_c in the 4–22 K range according to several authors.[1,2] The structure of this phase consists of double Bi–O layers alternating with single Sr–Cu–Sr perovskite sheets along the *c* axis. The second pseudoternary Bi–Sr–Cu–O phase has been recently discovered and characterized by our group, having the composition $Bi_4Sr_8Cu_4O_{19+y}$.[7-9] Figure 1 shows a perspective view of the cation sublattice (1a) and copper–oxygen framework (1b) for this oxide along with the atomic numbering scheme in the asymmetric unit (1c).

This new phase is not superconducting, although it shows close structural relationships with $Bi_2Sr_2CuO_{6+y}$. The main difference between both oxides is the presence in $Bi_4Sr_8Cu_5O_{19+y}$ of extra Sr–Cu–Sr perovskite layers arranged perpendicularly to the $[CuO_2]$ planes (i.e., perpendicular to the *b* axis), which break the two-dimensional character of the structure, common to all high-T_c superconducting copper oxides. This is a completely new structural network in the field of perovskites that may shed light in the central problem of the relevance of low dimensionality in high-T_c superconductivity.

In this paper we present the study of its crystal structure and physical properties by means of neutron powder diffraction, high-resolution electron microscopy, electrical resistivity, and magnetic susceptibility.

Experimental Section

Samples were prepared by using two different oxide percursor routes. In the first route, I, $Bi_2Sr_2CuO_6$ was used as starting material and prepared by firing in air at 850 °C a mixture of Bi_2O_3, SrC_2O_4, and CuO in stoichiometric amounts. Then, a 2:3:1 molar ratio of $Bi_2Sr_2CuO_6$, $SrCuO_2$, and SrC_2O_4 was subjected to a treatment involving several heatings in air at 900 °C during 48 h with intermediate regrindings. Portions of the sample prepared by this procedure (hereafter named AA) were further reannealed at 900 °C in flowing oxygen (sample OA). X-ray powder diffraction of this sample did not show any impurity phase.

In the second route, II, employed for the preparation of the sample ($\simeq$15 g) used in the neutron diffraction experiment, Bi_2CuO_4 was first prepared in air at 750 °C from Bi_2O_3 and CuO

* Author to whom correspondence should be addressed.
† Institut Max von Laue-Paul Langevin, 156 X, 38042 Grenoble Cedex, France.
‡ Laboratorio de Magnetismo Aplicado (RENFE-UCM), 28290 Las Matas, Madrid, Spain.

(1) Michel, C.; Hervieu, M.; Borel, M. M.; Deslandes, F.; Provost, J.; Raveau, B. *Z. Phys.* **1987**, *B68*, 421.
(2) Maeda, M.; Tanaka, Y.; Fukutomi, M.; Asano, T. *Jpn. J. Appl. Phys.* **1988**, *27*, L209.
(3) Subramanian, M. A.; C. C. Torardi, C. C.; Calabrese, J. C.; Goapalkrishnan, J.; Morrisey, K. J.; Askew, T. R.; Flippen, R. B.; Chowdhry, U.; Sleight, A. W. *Science* **1988**, *239*, 1015.
(4) Tarascon, J. M.; Le page, Y.; Barboux, P.; Bagley, B. G.; Greene, L. H.; McKinnon, W. R.; Hull, G. W.; Giroud, M.; Hwang, D. M. *Phys. Rev. B* **1988**, *37*, 9382.
(5) Bordet, P.; Capponi, J. J.; Chaillout, C.; Chenavas, J.; Hewat, A. W.; Hewat, E. A.; Hodeau, J. L.; Marezio, M.; Tholence, J. L.; Tranqui, D. *Physica C* **1988**, 153–155, 623.
(6) Sunshine, S. A.; Siegrist, T.; Schneemeyer, L. F.; Murphy, D. W.; Cava, R. J.; Batlogg, B.; Van Dover, R. B.; Fleming, R. M.; Glarum, S. H.; Nakahara, S.; Farrow, R.; Krajewski, J. J.; Zahurak, S. M.; Wasczczak, J. V.; Marshall, J. H.; Marsh, P.; Rupp, L. W. Jr.; Peck, W. F. *Phys. Rev. B* **1988**, *38*, 893.
(7) Fuertes, A.; Miravitlles, C.; Gonzalez-Calbet, J.; Vallet-Regi, M.; Obradors, X.; Rodriguez-Carvajal, J. *Physica C* **1989**, *157*, 525.
(8) Caldes, M. T.; Fuertes, A.; Gonzalez-Calbet, J. M.; Vallet-Regi, M.; Garcia, A.; Obradors, X.; Fontcuberta, J.; Rodriquez, J.; Miravitlles, C.; Perez, F. *Physica C* **1990**, 162–164, 5659.
(9) Caldes, M. T.; Navarro, J. M.; Fuertes, A.; Obradors, X.; Miravitlles, C.; Rodriguez-Carvajal, J.; Vallet, M.; Gonzalez-Calbet, J. In High-Temperature Superconductors: Fundamental Properties and Novel Materials Processing. *Mater. Res. Soc. Proc.* **1990**, *169*, 133.

0897-4756/91/2803-0844$02.50/0

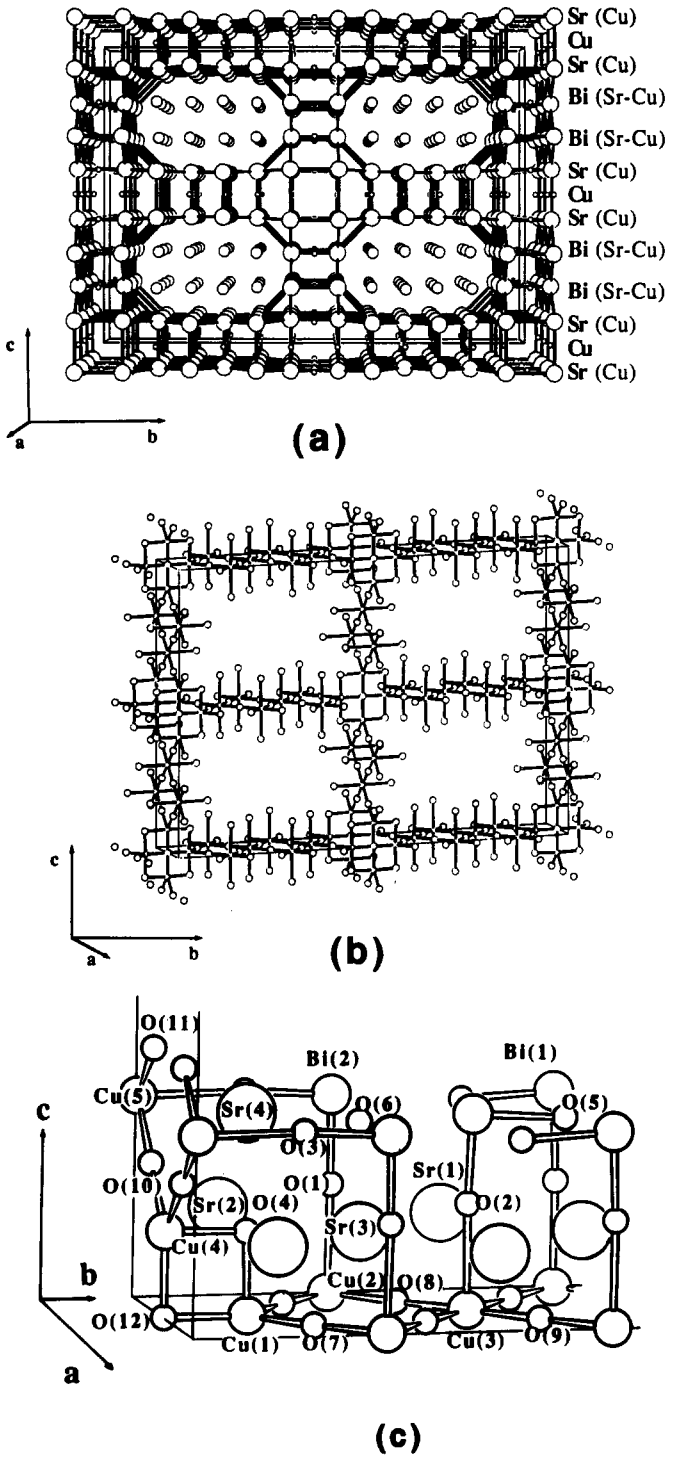

Figure 1. (a) Perspective view of the cation sublattice along [100] for $Bi_4Sr_8Cu_5O_{19+y}$. Atoms are represented as small (Cu), medium (Bi), and large (Sr) open circles. Lines join Sr atoms with interatomic distances less than 4.1 Å. (b) Copper–oxygen framework of $Bi_4Sr_8Cu_5O_{19+y}$ showing the large tunnels occupied by Bi–O rows. Copper atoms are small circles. (c) Atomic numbering in the asymmetric unit of $Bi_4Sr_8Cu_5O_{19+y}$.

in a molar ratio 1:1. Then, a mixture of Bi_2CuO_4, $SrCuO_2$, and SrC_2O_4 in 2:3:5 molar ratio was heated in air for 48 h and reannealed in the same atmosphere and at the same temperature during 120 h. X-ray powder diffraction of this sample showed up a very small amount of $SrCuO_2$ as an impurity phase.

Neutron diffraction experiments were performed at 1.5 and 300 K on the high-resolution powder diffractometer D2B at the I.L.L. in Grenoble. The step size for this experiment was 0.05° in 2ϑ. The explored angular range was 0–160° (2ϑ), and the preselected monitor counts, for a fixed position of the detector bank, was 100000. The neutron wavelength used in the refinement was 1.5945 Å. A neutron powder diffraction experiment as a function of temperature between 300 and 998 K was performed at the high-flux, medium-resolution D1B diffractometer also at the I.L.L. This diffractometer is equipped with a 400-cell position-sensitive detector (PSD), spanning an angualr range of 80° (2ϑ). The analysis of the data was performed using the programs of the STRAP package.[10] The data from the D2B were used for structure refinement starting with the previously reported atomic coordinates obtained from single-crystal X-ray diffraction study.[7] The structural parameters of the impurity phase $SrCuO_2$ were also included in the refinement using the positions given by Weller and Lines.[11]

Electron diffraction patterns were recorded in a JEOL 2000 F electron microscope equipped with a side-entry goniometer stage with tilt angles of ±45° and operating at 200 kV. High-resolution electron microscopy (HREM) was performed in a JEOL 4000 EX electron microscope equipped with a top-entry goniometer stage with ±25° tilt angle and operating at 400 kV. The sample was crushed in an agate mortar and dispersed in 1-butanol. Drops of the resultant suspension were collected on a perforated carbon film supported on a Cu grid.

Electrical resistivity measurements were carried out by the four-point method (1 mA) in the 60 K ≤ T ≤ 300 K temperature range. Seebeck measurements have also been performed in the same temperature range by using a homemade experimental setup. The magnetic susceptibility was measured down to 4 K on a Quantum Design SQUID magnetometer operating at 500 Oe and on a Lake Shore ac susceptometer operating at 10 Oe and 111 Hz.

Results and Discussion

Synthesis. $Bi_4Sr_8Cu_5O_{19+y}$ is obtained by using one of the two solid-state reactions, $2Bi_2Sr_2CuO_6 + 3SrCuO_2 + SrC_2O_4$ (route I) or $2Bi_2CuO_4 + 3SrCuO_2 + 5SrC_2O_4$ (route II). Direct solid-state reaction of Bi_2O_3, SrC_2O_4, and CuO requires very long reaction times, and we observe in the final product important amounts of impurity phases such as $Bi_2Sr_2CuO_6$ and different strontium copper binary oxides. Concerning route I and taking into account the crystal structures of the starting materials $Bi_2Sr_2CuO_6$ and $SrCuO_2$,[11-13] the reaction involves direct insertion of "CuO_2" planes in $Bi_2Sr_2CuO_6$, planes that in $Bi_4Sr_8Cu_5O_{19+y}$ are perpendicular to those existing in the 2201 material.[7] This kind of solid-state reaction based on starting materials with structural elements common to the final product has been demonstrated to be very useful for the stabilization of oxide phases with complex structures.[14,15] Concerning route II, Bi_2CuO_4 is used as a matrix precursor because it possesses an ideal open structure for the topochemical insertion of copper and alkaline-earth-metal ions in the preparation of $Bi_4Sr_8Cu_5O_{19+y}$. In this case, the reaction pathway is less direct than in route I, involving the formation of a phase of nominal composition $Bi_2Sr_3Cu_2O_8$[16] as an intermediate product.

High-Resolution Neutron Diffraction Study. Figure 2 shows the observed and calculated neutron powder diffraction pattern at room temperature for $Bi_4Sr_8Cu_5O_{19+y}$

(10) Rodriguez, J.; Anne, M.; Pannetier, J. *ILL Internal Report* **1987**, 87R0147.
(11) Weller, M. T.; Lines, D. R. *J. Solid State Chem.* **1989**, *82*, 21.
(12) Torrance, J. B.; Tokura, Y.; La Placa, S. J.; Huang, T. C.; Savoy, R. J.; Nazzal, A. I. *Solid State Commun.* **1988**, *66*, 703.
(13) Torardi, C. C.; Subramanian, M. A.; Calabrese, J. C.; Gopalakrishnan, J.; Mc Carron, E. M. C.; Morrisey, K. J.; Askew, T. R.; Flippen, R. B.; Chowdhry, U.; Sleight, A. W. *Phys. Rev. B* **1988**, *38*, 225.
(14) Beltran, D.; Caldes, M. T.; Ibanez, R.; Escriva, E.; Beltran, A.; Segura, A.; Munoz, V.; Martinez, J. *J. Less Common Met.* **1989**, *150*, 247.
(15) Fuertes, A.; Obradors, X.; Navarro, J. M.; Gomez-Romero, P.; Casan-Pastor, N.; Perez, F.; Fontcuberta, J.; Miravitlles, C.; Rodriguez-Carvajall, J.; Martinez, B. *Physica C* **1990**, *179*, 153.
(16) Ikeda, Y.; Ito, H.; Shimonura, S.; One, Y.; Inaba, K.; Hiroi, Z.; Takano, M. *Physica C* **1989**, *159*, 93.

Table I. Crystallographic Parameters

T	295 K	cell params, Å	
space group	$Fmmm$	a	5.3671 (1)
z	8	b	33.9719 (6)
		c	24.0722 (4)

atom coordinates	site	x	y	z	B, Å^2	occ
Bi(1)	16m	0	0.2883 (2)	0.1889 (2)	1.06 (4)	0.5
Bi(2)	16m	0	0.1343 (1)	0.1909 (3)	1.06 (4)	0.5
Sr(1)	16m	0	0.2112 (2)	0.0741 (2)	1.01 (4)	0.5
Sr(2)	16m	0	0.0573 (2)	0.0855 (3)	1.01 (4)	0.465 (8)
Sr(3)	16m	0	0.3652 (2)	0.0783 (3)	1.01 (4)	0.5
Sr(4)	16m	0	0.4455 (2)	0.1961 (3)	1.01 (4)	0.5
Cu(1)	8h	0	0.4422 (2)	0	1.02 (3)	0.25
Cu(2)	8h	0	0.1339 (2)	0	1.02 (3)	0.25
Cu(3)	8h	0	0.2901 (3)	0	1.02 (3)	0.25
Cu(4)	8i	0	0.5	0.0833 (3)	1.02 (3)	0.25
Cu(5)	8i	0	0	0.1947 (3)	1.02 (3)	0.25
O(1)	16m	0	0.1351 (2)	0.1047 (3)	1.48 (4)	0.5
O(2)	16m	0.5	0.2093 (2)	0.1026 (3)	1.48 (4)	0.5
O(3)	16m	0	0.0740 (2)	0.1963 (3)	1.48 (4)	0.5
O(4)	16m	0.5	0.0562 (2)	0.0813 (3)	1.48 (4)	0.421 (9)
O(5)	32p	0.3825 (17)	0.2753 (3)	0.1835 (4)	1.48 (4)	0.5
O(6)	32p	0.4018 (16)	0.1329 (3)	0.1845 (4)	1.48 (4)	0.5
O(7)	16o	0.235 (2)	0.0932 (3)	0	1.48 (4)	0.310 (8)
O(8)	16o	0.2541 (16)	0.1711 (2)	0	1.48 (4)	0.5
O(9)	8e	0.25	0.25	0	1.48 (4)	0.25
O(10)	16n	0.2394 (17)	0	0.1392 (4)	1.48 (4)	0.398 (8)
O(11)	8d	0.25	0	0.25	1.48 (4)	0.25
O(12)	8g	0.3575	0	0	1.48 (4)	0.136 (5)

number of reflections 1215
reliability factors R_p, 4.46; R_{wp}, 5.89; R_e, 1.45; R_{Bragg}, 6.08

Table II. Selected Interatomic Bond Distances (angstroms) for $Bi_4Sr_8Cu_5O_{19+y}$

Bi(1)–O(2)	2.081 (9)	Bi(2)–O(1)	2.075 (10)
Bi(1)–O(5)	3.346 (9)	Bi(2)–O(3)	2.053 (8)
Bi(1)–O(5)	2.104 (9)	Bi(2)–O(5)	3.140 (11)
Bi(1)–O(5)	2.255 (12)	Bi(2)–O(6)	3.215 (9)
Bi(1)–O(5)	3.164 (11)	Bi(2)–O(6)	2.163 (9)
Bi(1)–O(6)	2.731 (12)	Bi(2)–O(6)	3.046 (12)
Sr(1)–O(1)	2.688 (10)	Sr(2)–O(1)	2.683 (10)
Sr(1)–O(2)	2.771 (2) × 2	Sr(2)–O(3)	2.725 (10)
Sr(1)–O(2)	2.787 (10)	Sr(2)–O(4)	2.686 (4) × 2
Sr(1)–O(5)	2.747 (11)	Sr(2)–O(7)	2.704 (9) × 2
Sr(1)–O(8)	2.627 (7) × 2	Sr(2)–O(10)	2.667 (9) × 2
Sr(1)–O(9)	2.592 (5) × 2		
Sr(3)–O(1)	2.758 (2) × 2	Sr(4)–O(3)	2.764 (2) × 2
Sr(3)–O(2)	2.598 (10)	Sr(4)–O(3)	2.676 (10)
Sr(3)–O(4)	2.671 (10)	Sr(4)–O(4)	2.764 (10)
Sr(3)–O(6)	2.611 (12)	Sr(4)–O(6)	2.729 (12)
Sr(3)–O(7)	2.753 (10) × 2	Sr(4)–O(10)	2.695 (9) × 2
Sr(3)–O(8)	2.610 (8) × 2	Sr(4)–O(11)	2.629 (6) × 2
Cu(1)–O(4)	1.958 (7) × 2	Cu(2)–O(1)	2.521 (7) × 2
Cu(1)–O(7)	1.864 (11) × 2	Cu(2)–O(7)	1.870 (12) × 2
Cu(1)–O(12)	2.107 (9)	Cu(2)–O(8)	1.860 (9) × 2
Cu(3)–O(2)	2.470 (7) × 2	Cu(4)–O(4)	1.910 (7) × 2
Cu(3)–O(8)	1.867 (11) × 2	Cu(4)–O(10)	1.941 (11) × 2
Cu(3)–O(9)	1.910 (7) × 2	Cu(4)–O(12)	2.146 (9)
Cu(5)–O(3)	2.514 (7) × 2		
Cu(5)–O(10)	1.854 (11) × 2		
Cu(5)–O(11)	1.890 (5) × 2		

Table III. Selected Angles (degrees) for Copper Polyhedra in $Bi_4Sr_8Cu_5O_{19+y}$

O(4)–Cu(1)–O(4)	176.8 (5)	O(1)–Cu(2)–O(7)	90.7 (5)
O(4)–Cu(1)–O(7)	91.0 (6)	O(1)–Cu(2)–O(1)	178.5 (7)
O(4)–Cu(1)–O(12)	88.5 (4)	O(1)–Cu(2)–O(8)	89.4 (4)
O(7)–Cu(1)–O(7)	99.7 (9)	O(7)–Cu(2)–O(7)	84.6 (8)
O(7)–Cu(1)–O(12)	108.9 (8)	O(7)–Cu(2)–O(8)	90.5 (7)
O(7)–Cu(1)–O(12)	151.5 (8)	O(7)–Cu(2)–O(8)	175.1 (6)
		O(8)–Cu(2)–O(8)	94.4 (7)
O(2)–Cu(3)–O(2)	178.9 (6)	O(4)–Cu(4)–O(4)	177.1 (7)
O(2)–Cu(3)–O(8)	89.6 (5)	O(4)–Cu(4)–O(10)	91.0 (6)
O(2)–Cu(3)–O(9)	90.4 (4)	O(4)–Cu(4)–O(12)	88.7 (5)
O(8)–Cu(3)–O(8)	89.9 (7)	O(10)–Cu(4)–O(10)	92.2 (7)
O(8)–Cu(3)–O(9)	179.7 (6)	O(10)–Cu(4)–O(12)	113.0 (8)
O(8)–Cu(3)–O(9)	90.4 (5)	O(10)–Cu(4)–O(12)	154.8 (7)
O(9)–Cu(3)–O(9)	89.3 (3)		
O(3)–Cu(5)–O(3)	178.4 (4)		
O(3)–Cu(5)–O(10)	90.6 (5)		
O(3)–Cu(5)–O(11)	89.4 (3)		
O(10)–Cu(5)–O(10)	87.8 (7)		
O(10)–Cu(5)–O(11)	90.9 (6)		
O(10)–Cu(5)–O(11)	178.7 (6)		
O(11)–Cu(5)–O(11)	90.5 (2)		

(prepared by route II), measured on the high-resolution D2B powder diffractometer. Table I lists the crystallographic parameters, Table II selected interatomic bond distances, and Table III selected angles for copper polyhedra.

The atomic positions obtained from this experiment are very close to those reported from the single-crystal X-ray diffraction study.[7] The structure is described in the space group *Fmmm*, which implies a disordered model for the oxygen atoms O(5) and O(6) in the bismuth planes and for the oxygen atom O(12) (see Figure 1). The oxygen atoms in the bismuth planes are located in positions intermediate between NaCl and bridging sites.

There are, however, some reflections that cannot be indexed in *Fmmm* and that could be better fitted on the basis of a B-centered cell, requiring then an ordered model for those oxygens. In the *Fmmm* disordered model Bi(1) shows a distorted octahedral coordination very close to that found in superconducting $Bi_2Sr_2Ca_{n-1}Cu_nO_{2n+4}$.[17] Bi(2) is surrounded by a less distorted octahedron that Bi(1) due to its interaction with an oxygen atom belonging to the coordination polyhedron of Cu(5) in the perovskite layer along c.

Figure 3 shows the average structure in the Bi–O planes for the *Fmmm* model. If we consider only the Bi–O short bonds, the same zigzag chains of –Bi–O–Bi– that are

(17) Bordet, P.; Capponi, J. J.; Chaillout, C.; Chenavas, J.; Hewat, A. W.; Hewat, E. A.; Hodeau, J. L.; Marezio, M.; Tholence, J. L.; Tranqui, D. *Physica C* **1988**, *156*, 189.

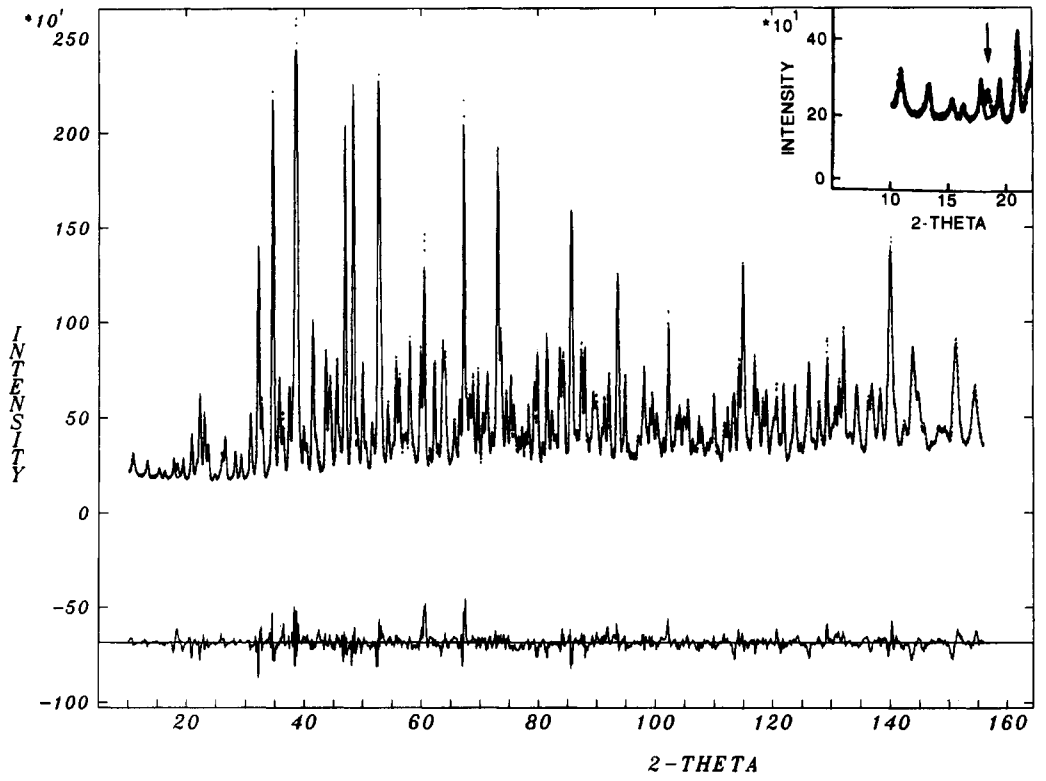

Figure 2. Experimental and calculated neutron diffraction patterns of $Bi_4Sr_8Cu_5O_{19+y}$. The inset shows one reflection not indexed in *Fmmm* that could be fitted on the basis of a B-centered cell.

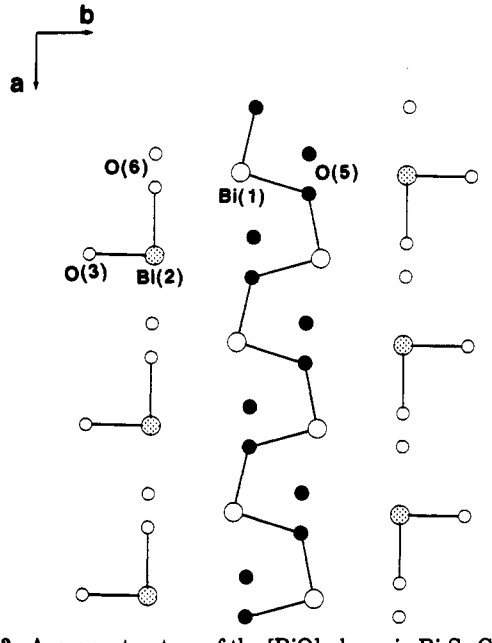

Figure 3. Average structure of the [BiO] planes in $Bi_4Sr_8Cu_5O_{19+y}$ showing Bi–O short bonds.

proposed for bismuth superconductors[17] can be considered for Bi(1). These chains, however, can be constructed only along the *a* axis, the direction of the Bi–O "tubes". In contrast, just the existence of isolated BiO_2 units with short Bi–O bonds may be considered for Bi(2).

Copper coordination geometries for Cu(2), Cu(3), and Cu(5) are tetragonally elongated octahedra. On the other hand, Cu(1) and Cu(4) have a coordination number of five since, in this disordered model, O(12) refines to two positions very close to each other (0.8 Å from the (100) plane) with partial occupancies $\simeq 1/2$ of that corresponding to the site symmetry. The geometrical arrangement for Cu(1) and Cu(4) consists of distorted trigonal bipyramids in which one of the corners corresponds to the disordered oxygen atom mentioned above. (Note that the average angles O(7)–Cu(1)–O(12) and O(10)-Cu(4)-O(12) are $\cong$130°.) It is worth mentioning that although trigonal bipyramidal coordination for copper is not common, some cases are known[18] even in extended solids as $Cu_2O(SO_4)$, $Cu_2(AsO_4)OH$, or Cu_3WO_6, where trigonal bipyramidal octahedral coordinations coexist. It is notable in those cases the distortion of the bipyramid.[19,20]

The octahedra share corners, as observed in La_2CuO_4, showing four distances Cu–O close to 1.9 Å and two weaker Cu–O bonds of about 2.5 Å. The two bipyramidal polyhedra show a similar distribution of distances, with two Cu–O bonds of around 1.90 Å, two of 1.95 Å, and the larger to the oxygen atom O(12) ($\simeq$2.1 Å). This atom is disordered along the *a* axis around the center of the cage formed as a result of the crossing of the two perovskite layers, being shared by four bipyramidal copper ions (two Cu(1) and two Cu(4)). Around Sr(1), Sr(3), and Sr(4) nine oxygen atoms define a face-capped cubic antiprism as in the case of La coordination polyhedron in La_2CuO_4, which can be described as resulting from the replacement of the four oxygens on the face of the cuboctahedron characteristic of the perovskite structure by a single oxygen. The oxygen polyhedron surrounding Sr(2) is a distorted cubic antiprism, very similar to the Ba polyhedron in $YBa_2Cu_3O_6$.

The refined stoichiometry was $Bi_4Sr_{7.86}Cu_5O_{19.06}$, which implies the existence of Sr and O vacancies in the structure. These vacancies are located in the cage formed by the crossing of the two perovskite layers where some disorder was expected.[7]

Bond valence sum calculations were performed following the method of Brown and Altermatt,[21] with a radius R_0 for

(18) Wells, A. F. *Structural Inorganic Chemistry*, 5th ed.; Clarendon Press: New York, 1984; pp 1117–1133.
(19) Toman, K. *Acta Crystallogr.* **1977**, *B33*, 2628.
(20) Gebert, E.; Kihlborg, L. *Acta Chem. Scand.* **1969**, *23*, 221.
(21) Brown, I. D.; Altermatt, D. *Acta Crystallogr. B* **1985**, *41*, 244.

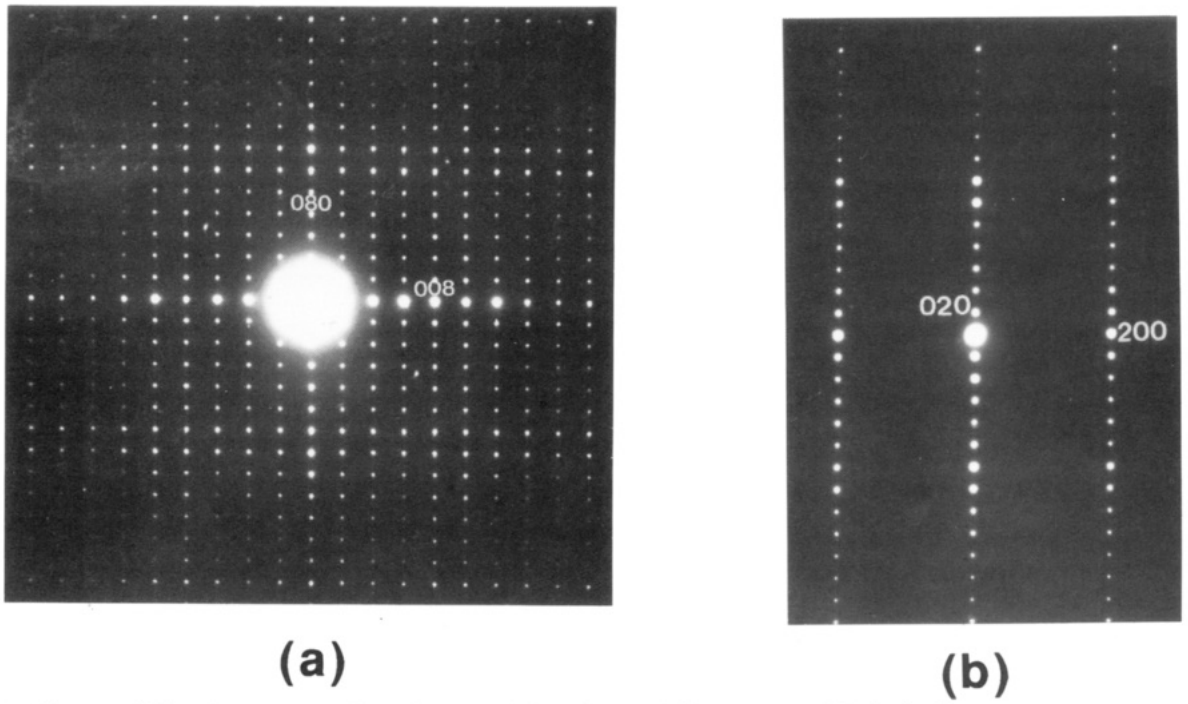

Figure 4. Electron diffraction patterns along the [100] (4a) and [001] (4b) zone axis of $Bi_4Sr_8Cu_5O_{19+y}$.

Table IV. Bond Valence Sums for Copper Ions in $Bi_4Sr_8Cu_5O_{19+y}$

	bond valence sum	
copper atom	method of ref 21 R_0: Cu^{2+}–O^{2-}	method of refs 22, 23 av R_0: Cu^{2+}–O^{21} R_0': $Cu^{+,3+}$–O^{2-}
bipyramidal		
Cu(1)	1.91	1.86
Cu(4)	1.99	1.99
octahedral		
Cu(2)	2.18	2.26
Cu(3)	2.52	2.84
Cu(5)	2.34	2.52
av Cu valence	2.19	2.29

Cu^{2+}–O^{2-}. Since Brown's correlations are known to deviate when the valence state changes, the calculation has been also done by the method of Brown and Tallon using both R_0 for Cu^{2+}–O^{2-} and R_0 for Cu^{3+}–O^{2-} if the valence comes above +2 or R_0 for Cu^{+}–O^{2-} if the valence comes below +2, and obtaining a weighed average of the bond valence sums as described elsewhere.[22,23] In both cases, partial oxygen occupancies were taken into account. The results obtained are summarized in Table IV.

Independently of the absolute bond valence sums obtained for each copper ion, or their error, both sets of data show a heterogeneous distribution of charges for coppers in different sites. Valences smaller or close to +2 are calculated for copper atoms in the bipyramidal positions at the crossing of layers. However, the valences for octahedral coppers are considerably larger than +2, with values increasing as the distance form the crossing increases. Then, there is a charge distribution within the cell, which rends reduced coppers in the connection of $[CuO_2]$ layers and oxidized copper ions in the positions far away from them.

Bond valence sums for Bi and Sr ions are internally consistent with the exception of that of Sr(2), which shows partial occupancy. Average bond valences for copper according to methods in refs 21 or 22 are 2.19 and 2.29, respectively, versus the value 2.08 calculated from atomic stoichiometry.

It seems then that the charge distribution within the $[CuO_2]$ layers stacked along c is originated by the pillaring of perpendicular $[CuO_2]$ layers, whose charge distribution, in turn, also gets changed. It is highly probable that the sharp change in transport properties observed when going from superconducting $Bi_2Sr_2CuO_6$ to $Bi_4Sr_8Cu_5O_{19+y}$ (see below) is originated in this new charge distribution.

The observance of insulating behavior (see below) led us to think about the possibility of long-range antiferromagnetic ordering, as observed in the insulating precursors of the high-temperature superconductors, i.e., La_2CuO_4[24] and $YBa_2Cu_3O_6$.[25] Due to the complex diffraction pattern of $Bi_4Sr_8Cu_5O_{19+y}$ and the small value of the magnetic moment per Cu^{2+} ion it may be difficult to detect any long-range magnetic ordering in this sample. We have, however, analyzed the diffraction patterns at temperatures from 1.5 K up to T = 998 K without obtaining any evidence of extra Bragg lines of magnetic origin nor any change in intensity of the crystallographic lines that could be related to three-dimensional magnetic ordering. (The absence of this type of ordering has been confirmed by μSR (muon spin rotation) experiments[32]). We also did not observe any relevant structural change in this temperature range. The only effect seen is that the thermal expansion is more important along the c axis than on the ab plane, as expected in view of the marked layered nature of the structure in this direction.

High-Resolution Electron Microscopy. Parts a and b of Figure 4 show the electron diffraction patterns along the [100] and [001] zone axes, respectively. These patterns and others obtained by tilting around both a^*, b^*, and c^* axes can be indexed on the basis of the orthorhombic unit cell. Extinctions are generally in agreement with the *Fmmm* space group. But some crystals did show reflexions

(22) Brown, I. D. *J. Solid State Chem.* **1989**, *82*, 122.
(23) Tallon, J. L. *Physica C* **1990**, *168*, 85.
(24) Vaknin, D.; Caignol, E.; Davies, P. K.; Fischer, J. E.; Johnston, D. C.; Goshorn, D. P. *Phys. Rev. B* **1989**, *39*, 9122.
(25) Tranquada, J. M.; Moudden, A. H.; Goldman, A. I.; Zolliker, P.; Cox, D. E.; Shirane, G.; Sinha, S. K.; Vaknin, D.; Johnston, D. C.; Alvarez, M. S.; Jacobson, A. J.; Lewandowski, J. T.; Newsman, J. M. *Phys. Rev. B* **1988**, *38*, 2477.

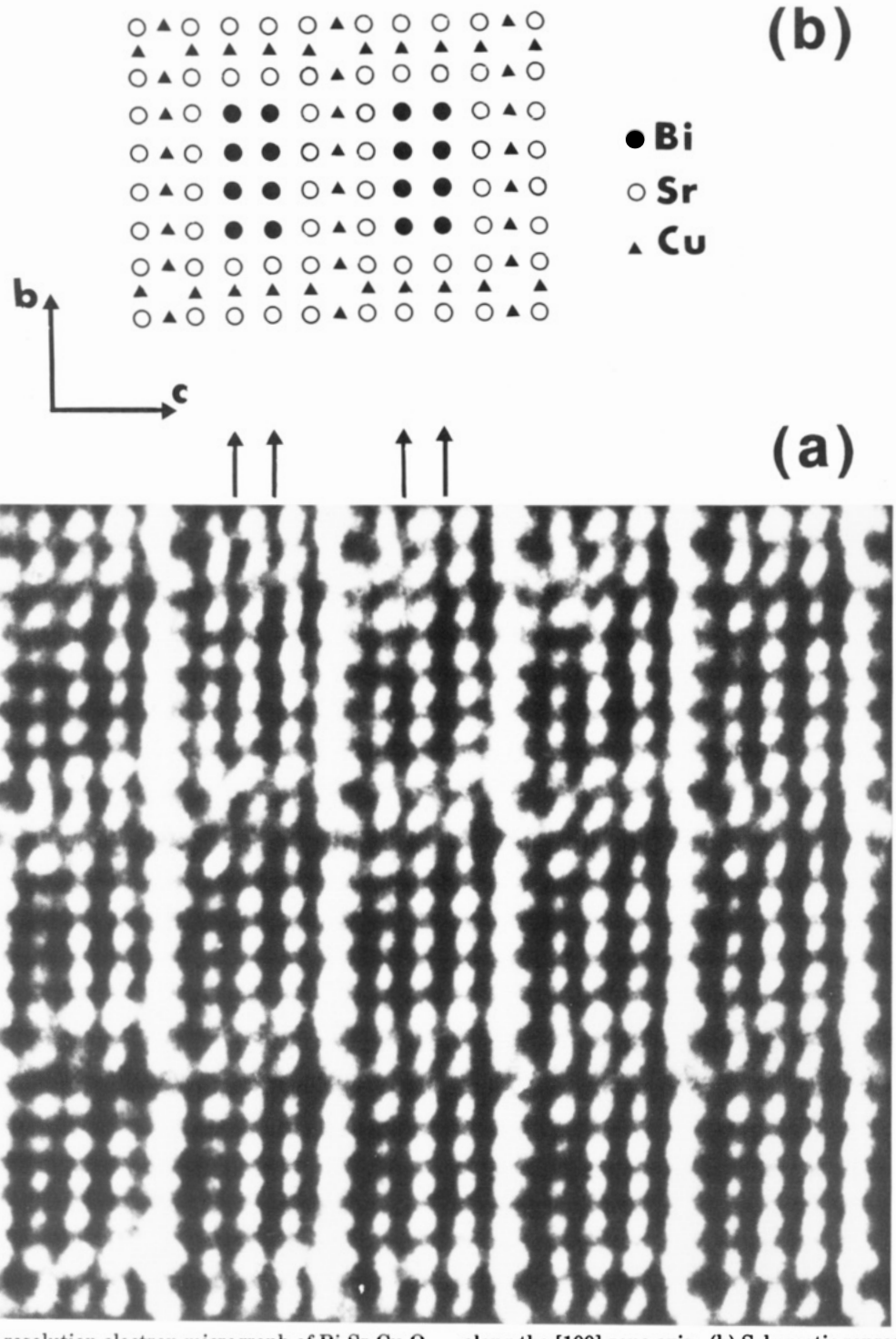

Figure 5. (a) High-resolution electron micrograph of $Bi_4Sr_8Cu_5O_{19+y}$ along the [100] zone axis. (b) Schematic representation of the cation sublattice along such a projection.

with $h,k,l = 2n + 1$, which may be caused by a lowering of the symmetry to a B-centered cell. Neither extra spots nor streaking of the diffraction maxima were observed, indicating that if compositional variations exist, they may be accommodated at random along the crystals. The existence of ordered crystals is confirmed in the corresponding structure images.

A high-resolution electron micrograph of the sample aligned with the short crystal axis ($\simeq$5.4 Å) parallel to the electron beam is seen in Figure 5a. The image can be interpreted comparing the observed contrast with the structure in the same figure. Thus, black dots following the vertical lines indicated by arrows correspond to double [BiO] layers. Bismuth atoms are represented by black dots in the schematic representation shown in Figure 5b. Every $\simeq$17 Å (i.e., = $b/2$) the four Bi double rows are separated by double layers containing Sr atoms. Such atoms correspond to all the black dots surrounding Bi atoms and are schematically represented (Figure 5b) by empty dots. Double layers of Sr are separated by copper atoms represented by small triangles, as can be seen in both Figure 5a and Figure 5b. A similar Sr–Cu–Sr layer is seen with $\simeq$12-Å separation following the c axis. The different contrast observed in both perpendicular Sr–Cu–Sr layers can be attributed to a slight misorientation of the crystal along [100] projection.

Despite the fact that neutron diffraction refinements show the oxygen atoms in $Bi_4Sr_8Cu_5O_{19+y}$ to be disordered

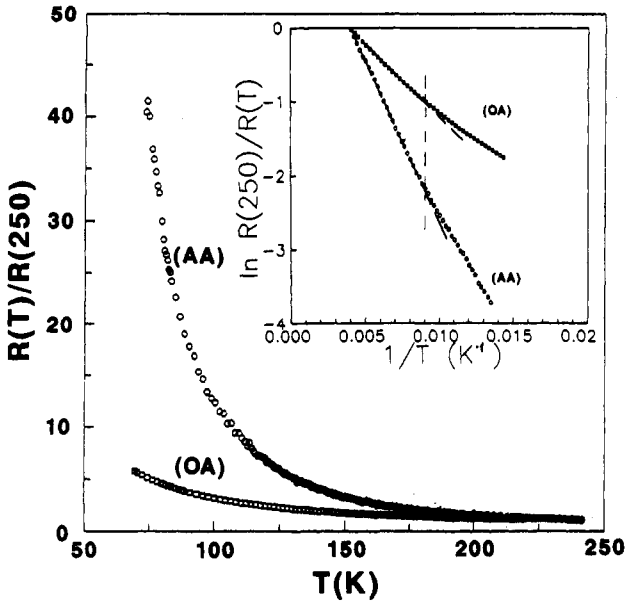

Figure 6. Electrical resistivity of $Bi_4Sr_8Cu_5O_{19+y}$. Inset: ln $[R(250)/R(T)]$ vs $1/T$. AA and OA refer to the air-prepared and oxygen-annealed samples, respectively.

in the Bi planes as it has also been observed for $Bi_2Sr_2Ca_{n-1}Cu_nO_{2n+4}$,[17] such disorder does not lead to the existence of a structural modulation as in the above series: the extra Sr–Cu–Sr perovskite layers perpendicular to the $[CuO_2]$ planes converts the layered $Bi_2Sr_2CuO_6$ structure into a rigid network preventing the corrugation of the [BiO] slabs and the modulation of the structure.[26]

In fact, taking into account the explanation given by Le Page et al. for the modulation of Bi superconductors,[26] the oxygen insertion in BiO_2 chains responsible of such modulation could still take place for $Bi_4Sr_8Cu_5O_{19+y}$ along the same chains in the a direction (i.e., along the Bi tunnels). However, the distortion involved by such insertion cannot apparently be accommodated by the rigid tubular structure.

Another possible origin for that modulation could be, as we suggested earlier,[7] the nearly periodic substitution of some Bi atoms by Sr along b, the tubular phase being a periodic example of such substitution.

Electrical Resistivity and Magnetic Properties. Electrical resistivity measurements in the 60 K < T < 300 K range showed semiconducting behavior for both the air- and oxygen-annealed samples (AA and OA, respectively). However, the room-temperature resistivity of sample AA (ρ(300 K) = 62.5 mΩ cm) is remarkably larger than the value for sample AO (ρ(300 K) = 21.2 mΩ cm). It is worth noticing that room-temperature resistivity for the OA sample is similar to that found in the basal plane of La_2CuO_4, for which ρ(300 K) = 13 mΩ cm.[27] Figure 6 shows the temperature dependence of $\rho(T)/\rho(250\text{ K})$ for both samples. It can be observed that linearity of log ρ vs $1/T$ exists only above ≃110 K. The conductivity activation energies for specimens AA and OA are $E_\rho \simeq 0.037$ and 0.017 eV, respectively.

At $T \leq 110$ K an appreciable lowering of slopes can be observed for both samples. The investigated low-temperature range is too narrow to attempt to infer any conduction mechanism; however, still using an activated model, values of $E_\rho \simeq 0.032$ and 0.011 eV are obtained for AA and OA, respectively. Such values are of the order of kT, and thus if E_ρ is considered as a mobility activation energy (E_μ), it follows that the energy barrier for charge transport for sample AA is only slightly larger than the thermal energy of carriers. A larger number of oxygen vacancies in the AA sample than in OA should be expected, which may also account for the smaller activation energy of the latter.

Seebeck measurements in the 70–300 K temperature range gave S(300 K) ≃ 30 (5) μV/K and increasing up to S(80 K) ≃ 40 (5) μV/K for the air-annealed sample, AA. Despite the fact that the small variation of the Seebeck coefficient in the investigated temperature range does not allow us to obtain an accurate estimation of the activation energy, the observed dependence $S(T)$ is consistent with a semiconducting-like behavior ($S \propto E_s/T$) of hole-type charge carriers. While scant attention should be paid to the exact E_s value, it is gratifying that $E_s \simeq 2$ meV is similar but smaller than E_ρ. Indeed, in a one-band model, $E_\rho > E_s$ is expected because of the mobility contributions to E_ρ. In the present case $E_\rho \simeq E_\mu + E_s \simeq E_\mu \simeq 30$ meV, thus implying that we are close to the itinerant charge carrier behavior. If one assumes that only the holes located in the basal plane contribute to the overall resistivity, their concentration being about 0.7 hole/formula unit, and that at 300 K all defects are exhausted, the room-temperature mobilities for OA and AA samples would be 0.2 and 0.08 $cm^2\ V^{-1}\ s^{-1}$, respectively. These small mobilities indicate that either the valence band is very narrow or some degree of localization is present. In conclusion, we observe that hole-type charge carriers have an activated mobility with an energy barrier that increases for the more oxygen-depleted samples. Indeed, hole-type conductivity was to be expected from the bond valence calculation results presented above.

In light of the present data it is obvious that the microscopic nature of the mobility barriers cannot be inferred. However, the fact that E_μ is larger for the more oxygen-deficient sample and the observation that oxygen vacancies are located at the crossing of the two perovskite layers (where the formal valence of copper ions is smaller or close to +2) lead to the suggestion that E_μ can be basically associated to the energy barriers that naturally occur at the perovskite blocks. If so, a mobility-activated conductivity along the b and c axes (see Figure 1) is to be expected.

In the absence of single crystals to measure ρ along the a axis (ρ_a), we can only conjecture that conductivity along this direction should be much higher and eventually of metallic type. It is obvious that the larger resistivity along the b and c directions would mask the ρ_a contribution, specially at low temperatures. Therefore, given the random nature of grain orientations in the ceramic sample, the resistivity would present a semiconductor-like behavior.

Magnetic susceptibility measurements were performed on sample AA at H = 500 Oe in the 4 K ≤ T ≤ 290 K temperature range. The observed behavior can be fitted to a law $\chi = \chi_0 + C/T$ with $\chi_0 = 1.23 \times 10^{-3}$ emu/mol and $C = 1.23 \times 10^{-1}$ emu K/g, corresponding to a 6–7% of free Cu^{2+} ions (see Figure 7). Similar values are obtained from the ac susceptometer data. Thus, we should conclude that the main contribution to the magnetic susceptibility, the χ_0 term, corresponds either to a metallic-like behavior or to the low-temperature tail of a strongly correlated antiferromagnetic system. The first possibility must be disregarded in view of the semiconducting behavior observed experimentally independent of the thermal treatments.

(26) Le Page, Y.; McKinnon, W. R.; Tarascon, J. M.; Barboux, P. *Phys. Rev. B* **1989**, *40*, 6810.
(27) Cheong, S. W.; Fish, Z.; Kwok, R. S.; Remeika, J. P.; Thompson, J. D.; Gruner, G. *Phys. Rev. B* **1988**, *37*, 5916.

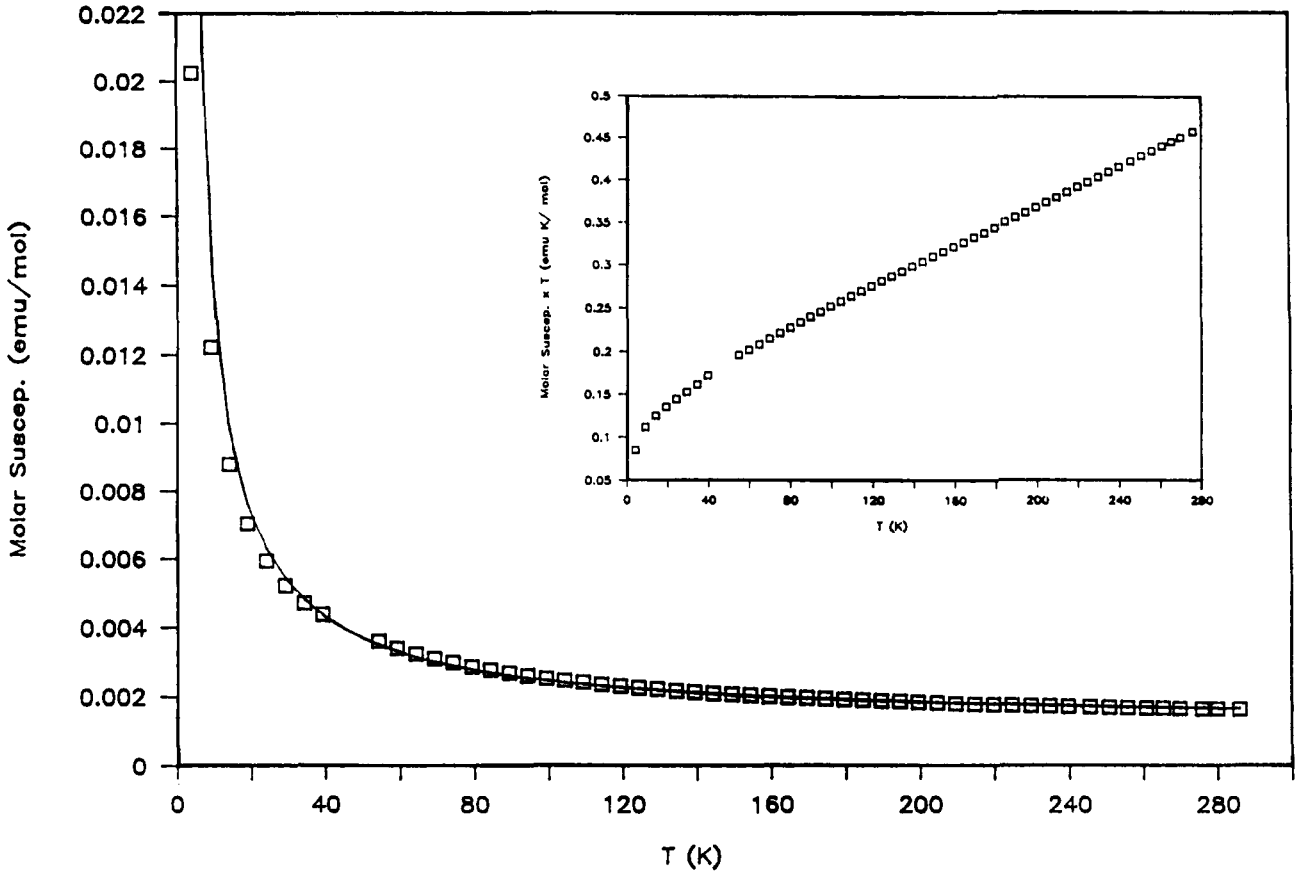

Figure 7. Magnetic susceptibility of $Bi_4Sr_8Cu_5O_{19+y}$. Inset shows the product χT vs T.

The second possibility, considering the lack of three-dimensional antiferromagnetic ordering evidenced by neutron diffraction and μSR experiments, involves low-dimensional antiferromagnetic behavior for the tubular phase. Such behavior could be similar to that observed in copper oxides having strong two-dimensional magnetic character such as $La_{2-x}Sr_xCuO_4$,[28] $YBa_2Cu_3O_{6+y}$,[25,29,30] or $(Ca,Sr)CuO_2$.[24] It appears in these systems that a very strong intraplane antiferromagnetic superexchange interaction J leads to extended 2D antiferromagnetic correlations,[31] and thus the susceptibility shows the features typical of 2D Heisenberg model, i.e. the $\chi(T)$ curve has a maximum at about 800 K ($J \simeq$ kT), remaining approximately constant below $T \sim 300$ K. For those compounds the existence or not of a long-range 3D antiferromagnetic ordering, as detected by neutron diffraction or μSR experiments, depends only on the hole concentration (which changes the extent of 2D antiferromagnetic correlations) and on the weak interlayer exchange interaction, which makes possible the crossover from 2D to 3D magnetic behavior.

From a structural point of view, the tubular phase, $Bi_4Sr_8Cu_5O_{19+y}$, has features strongly resembling those of the two-dimensional copper oxides, and thus it was expected that this compound would present as well strong antiferromagnetic correlations. No long-range 3D antiferromagnetic ordering has been detected, however, up to now, by either neutron diffraction or muon spin rotation.[32] It remains, then, to be investigated in which extent this is due to the hole doping we have already described above or to the breaking of the bidimensionality associated to the perpendicular perovskite planes.

The paramagnetic Curie-like susceptibility that dominates the observed susceptibility at low temperature is equivalent to the existence of 6–7% Cu^{2+} ions ($S = {}^1/_2$, $g = 2$) per formula unit. It is remarkable that similar Curie-like terms have already been observed for the antiferromagnetic insulator parent compounds of copper oxide superconductors.[30] The origin of this paramagnetic contribution has been largely discussed for the antiferromagnetic $YBa_2Cu_3O_6$. In such case it was concluded that a contribution coming solely from impurities is very unlikely.[30] It seems more plausible that some magnetic defects within the underlying antiferromagnetic lattice could originate the Curie-like paramagnetism.

In our case χT tends to zero as T is lowered, indicating that antiferromagnetic coupling with smaller J values is operating for the Cu^{2+} paramagnetic-like ions. According to the crystal structure such possibility is highly probable, since there are two types of Cu ions, octahedral and bipyramidal, involving different types of Cu–O–Cu overlaps. Some of those overlaps, such as Cu(bipyramidal)–O–Cu(octahedral), are expected from geometric considerations to be weaker than, for example, Cu(octahedral)–O–Cu(octahedral). It appears then likely that some Cu^{2+} ions remain magnetically decoupled around crystallographic defects such as oxygen or Sr vacancies. The existence of these "magnetic defects" has also been detected by means of specific heat measurements[33] where low-temperature

(28) (a) Birgeneau, R. G.; Shirane, G. In *Physical Properties of High Temperature Superconductors*; Gingsgerg, D. M., Ed.; World Scientific: London, 1989; Vol. I, and references therein. (b) Takegi, H.; Ido, T.; Utoa, M.; Uchida, S.; Tokura, T. *Phys. Rev. B* **1989**, *40*, 2254.

(29) Farneth, W. E.; McLean, R. S.; McCarron, III, E. M.; Zuo, F.; Lu, Y.; Patton, B. R.; Epstein, A. J. *Phys. Rev. B* **1989**, *39*, 6594.

(30) Obradors, X.; Tejada, J.; Rodriguez, J.; Perez, F.; Vallet, M.; Gonzalez-Calbet, J.; Medarde, M. *J. Magn. Mater.* **1990**, *83*, 517 and references therein.

(31) Johnston, D. C. *Phys. Rev. Lett.* **1989**, *62*, 957.

(32) Martinez, B.; Ansaldo, E. J. Private communication.

tails were correlated with the existence of Curie-law terms in the magnetic susceptibility of $YBa_2Cu_3O_{7-y}$.

Conclusions

Although the local atomic arrangements have close similarities with the structure of the superconducting oxides of the same system, the tubular phase shows an essential difference from all previously reported copper oxide superconductors: the $[CuO_2]$ planes are periodically interrupted by other $[CuO_2]$ planes stacked perpendicularly to them.

The most striking structural consequence of the insertion of such "perpendicular" $[CuO_2]$ planes is the absence of the typical structural modulations associated to the superconductors in the related series $Bi_2Sr_2Ca_{n-1}Cu_nO_{2n+4}$. This feature makes the tubular structure an ideal host lattice to study precise structural and crystalochemical changes derivated, for instance, from atomic substitutions or treatment under different atmospheres in order to compare them with those operating in the bismuth cuprate superconductors. Another important probable consequence of the crossing of two perovskite layers is the existence of a heterogeneous charge distribution among copper ions. This charge distribution may be responsible for the sharp change in transport properties observed when going from superconducting $Bi_2Sr_2CuO_{6+y}$ to $Bi_4Sr_8Cu_5O_{19+y}$. In particular, the charge modulation existing in the basal plane reduces the hole mobility, eventually giving rise to a localization at lower temperatures, and, thus, precluding the observation of metallic behavior.

The magnetic susceptibility of these insulating $Bi_4Sr_8Cu_5O_{19+y}$ samples appears to be consistent with that of a strongly correlated 2D antiferromagnetic Heisenberg model. No long-range 3D antiferromagnetic ordering has been observed, however, by either neutron diffraction or muon spin rotation. It would be worthwhile then to fully investigate the magnetic properties of this so-called "tubular" phase as a function of the hole doping. This will help in our understanding of the relationship existing among magnetic order and the insulator–metal transition observed in the layered superconducting copper perovskites.

Acknowledgment. We thank Dr. Pedro Gomez-Romero and Fernando Sapina for helpful discussions. This work has been supported by Grants from the Spanish CICYT (MAT88-0163-C03 and MAT90-1020-C02-01) and from the MIDAS program.

Registry No. $Bi_2Sr_2CuO_6$, 113924-17-7; Bi_2O_3, 1304-76-3; SrC_2O_4, 814-95-9; CuO, 1317-38-0; $SrCuO_2$, 57348-57-9; $Bi_4Sr_8Cu_5O_{19}$, 126653-12-1; Bi_2CuO_4, 39368-32-6.

(33) Junod, A. In *Physical Properties of High Temperature Superconductors*; Ginsberg, D. M., Ed.; World Scientific: London, 1990; Vol. II.

Benzospiropyrans as Photochromic and/or Thermochromic Photoinitiators

Suk-Kyu Lee and D. C. Neckers*

Center for Photochemical Sciences,[1] Bowling Green State University, Bowling Green, Ohio 43403

Received March 8, 1991. Revised Manuscript Received June 5, 1991

Iodinated merocyanines formed from the benzospiropyrans initiate radical photopolymerizations in the presence of co-initiators including tertiary amines and cetylpyridinium *n*-butyltriphenyl borate (CPB) when irradiated with a He/Ne (632 nm) or argon ion (514 nm) laser. The colored merocyanines were formed by one of four different methods: (1) by neutralization of the respective hydrochloric acid salts with tertiary amines; (2) by irradiation (360 nm) of the benzospiropyrans, (3) by dissolution of benzospiropyrans in *N*-vinylpyrrolidone; (4) by heating the benzospiropyrans.

Introduction

Benzospiropyrans (BSP) are an important class of compounds that undergo reversible intramolecular transformations (Scheme I[2]) forming the merocyanine (colored) isomer either by UV irradiation (photochromic) or by heating (thermochromic).

Our interest in the photoreactions of the BSPs is centered on the utilization of their colored/merocyanine forms as visible light photoinitators. The original notion was to generate a merocyanine from an appropriate benzospiropyran by irradiation and develop specific conditions wherein only radiation from a wavelength absorbed by the merocyanine effected photopolymerization. Rapid reversal of the merocyanine to the benzospiropyran might form the basis of a photochromic, two-photon-photoinitiator system such that polymerization would occur only at a point where two different light sources, one ultraviolet and the other visible, intersected.

Scheme I

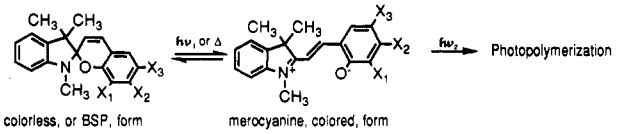

A previous attempt to utilize merocyanines as visible light photoinitiators was unsuccessful.[3] However, the

(1) Publication No. 109 from the Center for Photochemical Sciences.
(2) Tamaki, T.; Sakuragi, M.; Ichimura, K.; Aoki, K. *Chem. Phys. Lett.* **1989**, *161*, 23 and references therein.
(3) Bertelson, R. C.; Becker, W. J. *Research Study on the Application of the NCR Capsular System*; Rept. ASD-TR-61-325, Aug 1961, AD 265564; pp 59–60.

0897-4756/91/2803-0852$02.50/0